Near-Field Microwave Microscopy of Thin Film Resonators

J.A. Herbsommer, H. Safar, P.L. Gammel, B.P. Barber, and M. Zierdt

Bell Laboratories, Lucent Technologies, Murray Hill, NJ 07974

***Abstract* — We present phase-sensitive, high spatial resolution, near-field microwave microscopy images of the rf fields radiated by piezoelectric resonators operating in the vicinity of 2GHz. Near the resonance our data show a complex distribution of fields. We fit our data to the Butterworth/Van-Dyke model that describes the behavior of these devices, and find very good qualitative agreement. In general, we show the potential of this phase-sensitive near-field imaging technique to study the behavior of complex rf devices, with potential impact on the optimization of the device's design.**

I. Introduction

Modern rf devices and IC's require a complex optimization of their electrical properties, such as impedance, losses, etc. Crucial to this process are software modeling tools that allow to simulate the behavior of the device in the frequency window of interest. These models can produce a wealth of information, such as scattering parameters, field distribution, etc. While modeled scattering parameters can be readily compared to measurements, there exist the need of experimental tools that allow a direct, spatially resolved measurement of the device's properties.

In this paper we present, for the first time, scanning measurements of the local magnitude and phase of the fields radiated by a rf device, a thin-film resonator, [1] by using a phase-sensitive near-field microwave microscope. We have studied the spatial distribution of fields as a function of the frequency of the input power. The spatial maps of the phase and magnitude of the radiated fields show clear information of the device's behavior near its resonance's. We compare our data to the Butterworth/Van-Dyke (BVD) model [2] for piezoelectric resonator behavior. Together, our data and analysis demonstrates the potentials of this technique for the study of complex rf devices.

II. Experimental Details

Figure 1 shows a sketch of the experimental setup. The device under study is placed on a computer-controlled X-Y translation stage with 0.25μm minimum step size. The fields radiated by the device under study are detected using a custom open-coax tip, made using a tapered Tungsten microelectrode [3] covered with Kapton insulation that terminates in a sharp, 2 μm diameter tip. To complete the coax the microelectrode was tightly fit inside a thin Cu tube. We achieve simultaneous detection of the magnitude and phase of the radiated fields by using a Vector Network Analyzer (VNA) in our detection loop. One port of the VNA is used to drive the device, while the other port measures the fields detected by our coaxial tip. In this set-up, the cable's length and loss are easily accounted for in a through calibration, and a small electrical delay is used to correct the phase when the tip is connected as a detector.

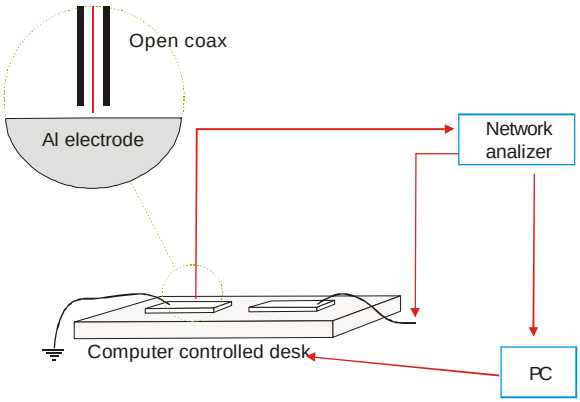

Figure 1: Experimental set-up.

As proposed by Vlahacos et al. [4] the detection of the perpendicular electric field is possible by capacitive coupling between the sample and the inner conductor of the tip. In fact, the radiated electric field induce a net charge on the inner element of the microprobe and modify its electric potential. While it is possible to model the capacitive interaction by taking into account the full geometry of the real system as discussed by Gao et al., [5] here we restrict to the parallel plate approximation, valid when the distance between the tip and the sample is equal or smaller than the diameter of the tip, as in our case. In this limit the spatial resolution is given by the largest of the diameter of the inner cable and the separation between the surface and the tip. [6] In our experiment the 2μm diameter tip was placed approximately 2μm from the sample surface, giving us a spatial resolution of 2 to 4μm.

0-7803-6540-2/01/$10.00 (C) 2001 IEEE

Previous work using the near-field microwave microscope technique concentrated mostly in the study of the dielectric properties of materials [7] and the behavior of simple devices such as strip-line resonators. [8] In all cases, these experiments concentrated only in the magnitude (power) of the radiated fields.

In this work we concentrate on the study of bulk mode thin film resonators (TFR), [1] an alternative to conventional miniature filters (e.g. SAW's). While substantial progress has been made in TFR design and fabrication, the problem of distribution of fields and currents in these devices remains as an open question. In fact, losses through the substrate, surface resistance of the electrodes, and parasitics due to packaging and geometry of the devices are factors that can affect the quality factor Q, bandwidth and the insertion loss of the filter applications. To address these issues it is necessary to perform spatially resolved measurements that can complement software simulations studies. Given the complexity of the TFR devices, with multiple near-by resonances, the capability of our set-up to measure the phase of the radiated fields becomes very important for a complete understanding of the device's properties.

III. Results

To demonstrate the performance of our microscope we first image the fields radiated by a Cu microstrip resonator.

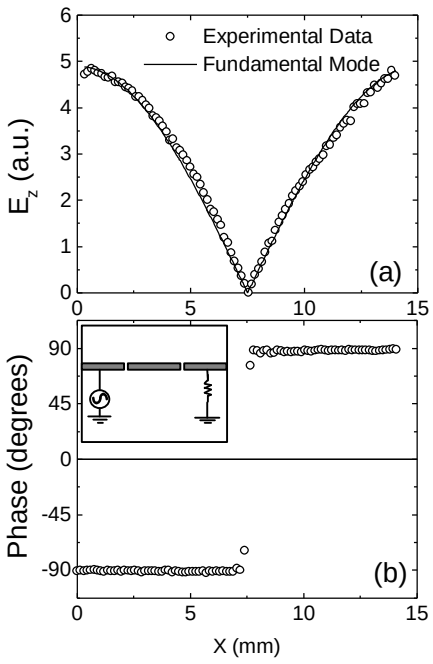

Figure 2: Magnitude (a) and phase (b) of the field radiated by a stripline resonator

The 15mm long Cu strip was excited through capacitive coupling with similar strips as shown in the inset of Fig. 2b). The frequency of resonance of the fundamental mode of the microstrip is at 2GHz. The scanning was performed along the center of the strip. In Fig. 2a) we show in open circles the measured perpendicular electric field and in solid line a fit to the expression expected for the electric field in the fundamental mode. For the phase it is expected a jump by 180^o at the position of the node, in excellent agreement with our experimental observation, as shown in Fig. 2b).

It should be noted that we observe no shift in the resonant frequency of the microstrip when our tip is placed nearby, indicative of the weak coupling between the tip and device. [7,8] We achieved this low coupling by minimizing the dimensions of the coax tip we use, not only the tip itself but also the ground layer of our coax.

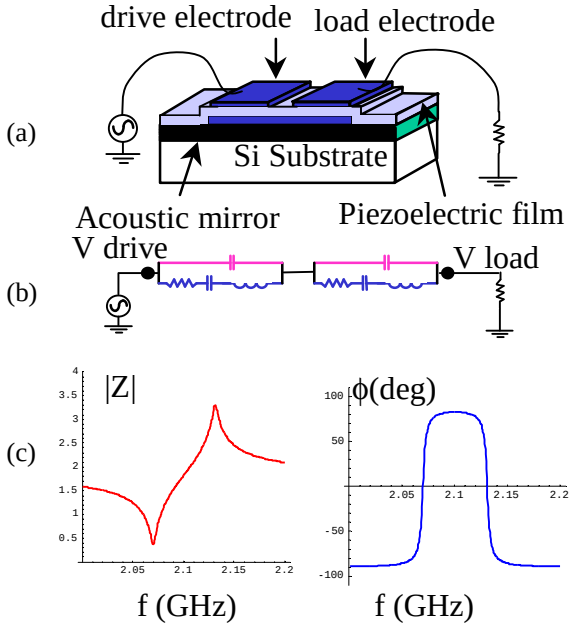

Figure 3: (a) sketch of a TFR, (b) BVD equivalent circuit, (c) Impedance and phase vs. frequency curves for the BVD model

We now turn to the measurements in TFR's. In Fig 3a) we show a sketch of a TFR device: an AlN film lays between a bottom Al electrode and two top electrodes . The dimension of the top electrodes of the device considered in this work were 80μm x 100μm. This design results in a series of two resonators, through the bottom electrode. Below this structure there is a stack of successive low and high acoustic impedance layers that act as a mirror to confine the acoustic energy in the device. All these structures were grown over a silicon substrate. To operate this device we connected one of the top electrodes to a rf input source, with the other connected to ground through a 50Ω termination.

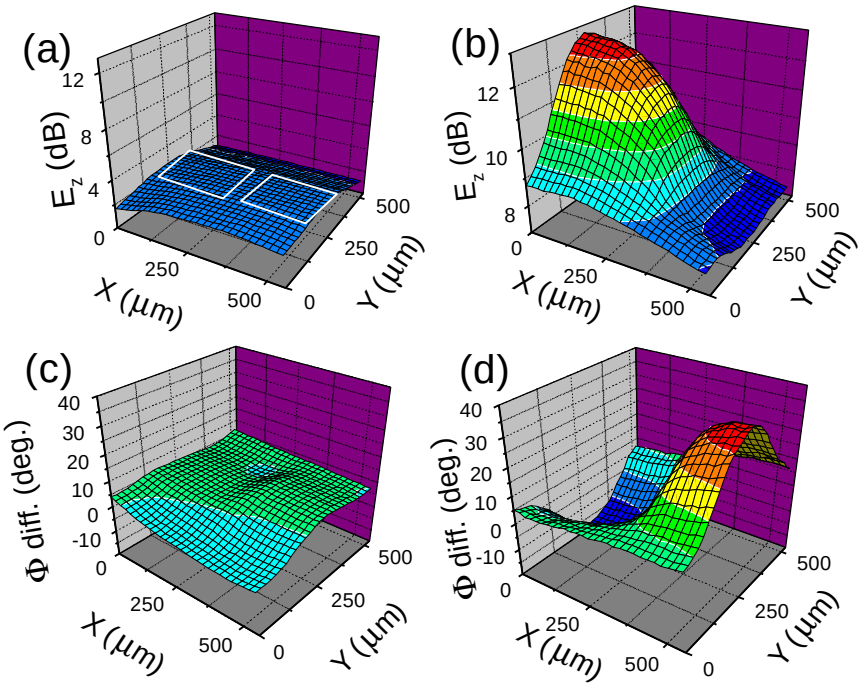

Figure 4: (a) Magnitude of the radiated field at 1.776GHz (zero's frequency) The lines in the figure indicate the electrode's position (drive electrode on the left-hand side of the figure), (b) Magnitude of the radiated field at 1.806GHz (pole's frequency), (c) Phase of the radiated field at 1.776GHz, (d) Phase of the radiated field at 1.850GHz (out of band).

The basic electrodynamic behavior of a single resonator is well described by the BVD model [2], which consists in the electrical equivalent circuit shown in Fig. 3b). A single resonator is represented by a parallel RLC circuit in which the upper branch represents the geometrical capacitance and the lower branch models the piezoelectric behavior. By choosing appropriately the values of all the components, this circuit describes well the frequency-dependent electrical impedance Z of the device, shown in Fig. 3c) as calculated from the BVD model with typical parameters for our devices. The phase curve shown in Figure 3cshows two frequencies at which the phase drop across the device is zero. The low frequency resonance (f_z) is called the 'zero' where the magnitude of the impedance reaches a minimum, and a high frequency resonance (f_p) called "pole" where Z reaches a maximum. In the case of the device studied here f_z=1.770GHz and f_p=1.804GHz, as determined from independent measurements of the scattering parameters. We note that away from resonance the device is capacitive (phase<0) and between the zero and pole frequencies the impedance is inductive (phase>0).

We have measured the spatial distribution of radiated fields for 200 frequencies between 1.6 and 1.9GHz at constant drive power. We find interesting changes in the distribution of the magnitude and phase of the radiated fields, in particular frequencies between the zero and the pole. To illustrate this behavior we show in Fig 4 the spatial distribution of the magnitude and phase of the radiated field for selected frequencies. Shown in Figure 4a) is the spatial distribution of the magnitude of the radiated field at the zero's frequency. We see that the radiated field has equal magnitude over both drive and load electrode, expected from the nearly zero impedance of the device at this frequency. However, at the pole's frequency we see a much higher magnitude of radiated field on the drive electrode. This behavior results from the high impedance of the device at this frequency. The spatial maps of the phase of the radiated field provide further proof for our description. Shown in Figure 4c) is the map of the phase of the radiated field at the zero's frequency. We see nearly no phase change across the drive and ground electrode, indicative of the practically pure resistive impedance of the device at this frequency. For frequencies away from the zero-pole window, we see in Figure 4d) that there is a phase drop between electrodes consistent with the capacitive nature of the device at these frequencies.

To illustrate the potential of our spatially resolved, phase sensitive technique we will analyze the difference in field magnitude and phase measured at the center of each of the top electrodes. In particular, we will quantitatively compare our data with the predictions of the BVD model. Within the parallel plate approximation, the measured radiated field is proportional to the electric potential at each of the two points considered at the *drive*

and *load* electrodes as noted by dots in Figs. 2a) and 2b). To avoid proportionality constants we consider the ratio V_d/V_l and the phase difference ϕ_d-ϕ_l. We now compare our measurement of V_d/V_l and ϕ_d-ϕ_l with the predictions the BVD model for two resonators connected in series terminated 50Ω, as shown in Fig. 3b). To better describe our data, we added to the model the impedance of the wire bond used to connect the device.

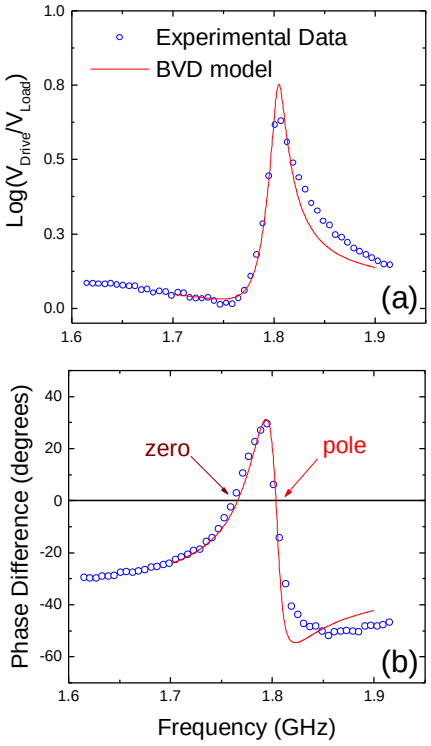

Figure 5: Fit of our data (shown with open circles) in magnitude (a), and phase (b) to the BVD model (solid line).

Shown in a) is the frequency dependence of the experimentally determined ratio V_d/V_l (in open circles) compared to the BVD model (solid line), showing very good agreement. For this fit we used parameters that are consistent with the values obtained from independent electrical characterization of the device. Other than purely geometrical parameters, our fit was done using 1.760GHz and 1.806Ghz for the zero and pole frequencies respectively, and a quality factor Q~200 for the pole resonance. This rather low Q (when compared to the ~300 value obtained from electrical measurements) may indicate tip-device coupling, as discussed later in this paper.

It is simple to explain the overall frequency dependence of the magnitude Vd/V_l. We find a minimum and a maximum exactly at the frequencies f_z and f_p respectively. The minimum, when the curve practically reaches zero, means that the voltages at both electrodes has the same value. This is because at f_z the impedance Z is small and all the voltage drops in the 50Ω termination. In contrast, at f_p when Z becomes large all the voltage drop occurs between the plates of the drive resonator. Shown in Fig 5b) is the phase difference between the drive and load electrodes. In open circles we show the experimental data and in full line the fit to the BVD model. Again, we find very good agreement. Both curves cross the horizontal axis at exactly the zero and pole frequencies, f_z and f_p, expected because at the resonant frequencies the device is purely resistive. Out of band, our data also shows the expected capacitive behavior, while inductive in-band.

It is interesting to note that the differences between our data and the model occur in the vicinity of the pole frequency. This may be attributed to a tip-device coupling effect, neglected in our analysis. Near the pole the device has electrical impedance well in the kΩ range, and our tip may be providing an alternative path to ground at this frequency range. These effects can be included in our model, and also minimized by an improved engineering of the tip.

IV. Conclusions

In conclusion, we have developed and implemented a phase-sensitive near field microwave microscope technique to measure the magnitude and phase of the electric fields radiated by rf devices. We demonstrated its use for the case of thin-film piezoelectric resonators. We have obtained spatial maps of the magnitude and phase of the radiated fields over a wide frequency range, including the resonant frequencies of these devices. We have compared the local response of the complex fields on different electrodes to the predictions of the BVD model and found very good agreement for the frequency dependence of both the magnitude and phase of the radiated fields. In general, our results show that it is an excellent spatially-resolved technique to study the behavior of complex rf devices.

V. References

1. K.M. Lakin et al., IEEE Trans. Microwave Theory and Tech., **41**, 2139 (1993)
2. S.Butterworth, Proc. Phys. Soc. **27**, 410-424 (1915); K.S.Van Dyke Proc. I.R.E. **16,** 742-764 (1928).
3. World Precision Instruments, Inc wpi@wpiinc.com
4. C.P.Vlahacos et al., App. Phys. Lett. **72,** 14, 1778 (1998).
5. C. Gao et al., App. Phys. Lett **75**, 19, 3005 (1999).
6. C.P.Vlahacos et al., App. Phys. Lett. **69,** 21, 3272 (1996).
7. Steinhauer et al., App. Phys. Lett **75**, 20, 3180 (1999), Y. Cho et al., App. Phys. Lett. **72,** 14, 1778 (1998).
8. C.P.Vlahacos et al, App. Phys. Lett. **73**, 17, 2491 (1998); S.K. Dutta et al., App. Phys. Lett. **74**, 1, 156 (1999).